Solid State Ionics 368 (2021) 115700

Contents lists available at ScienceDirect

Solid State Ionics

journal homepage: www.elsevier.com/locate/ssi

$SrTiO_3$ based high temperature solid oxide solar cells: Photovoltages, photocurrents and mechanistic insight

Maximilian Morgenbesser [a], Alexander Schmid [a,*], Alexander Viernstein [a], Juan de Dios Sirvent [b], Francesco Chiabrera [b], Niklas Bodenmüller [a], Stefanie Taibl [a], Markus Kubicek [a], Federico Baiutti [b], Albert Tarancon [b,c], Jürgen Fleig [a]

[a] TU Wien, Institut für chemische Technologien und Analytik, Getreidemarkt 9EC, 1060 Wien, Austria
[b] Catalonia Institute for Energy Research (IREC), Jardins de Les Dones de Negre 1, Sant Adria del Besos, Barcelona 08930, Spain
[c] ICREA, 23 Passeig Lluis Companys, Barcelona 08010, Spain

ARTICLE INFO

Keywords:
Photovoltage
Strontium titanate
High temperature solar cells
All oxide solar cells
Self enhancement effect

ABSTRACT

High temperature solid oxide solar cells based on $SrTiO_3$ (STO) are investigated. Schottky contacts between STO and different materials, including $La_{1-x}Sr_xCrO_3$, $La_{0.8}Sr_{0.2}MnO_3$, $La_{0.6}Sr_{0.4}CoO_3$ and metals like Au and Pt are illuminated by UV light with a wavelength of 365 nm at 350 °C in air and the resulting voltages and currents are measured. With certain material combinations, e.g. $LaCrO_3$/STO or Au/STO heterojunctions, high photovoltages of more than 1.0 V are obtained. Current measurements reveal changes in the bulk STO due to stoichiometry polarization, leading to a self-enhancement effect of the photovoltaic cell. Mechanistic insight in the processes under UV light is gained by electrochemical impedance spectroscopy, especially regarding the space charge region at the heterojunction and bulk changes due to stoichiometry polarization. In addition to the electronic effects upon illumination, also photo-ionic effects of oxygen transport caused by chemical potential changes were observed.

1. Introduction

Finding clean and sustainable ways of providing energy is a major challenge of the 21st century with global problems such as climate change and air pollution. One promising approach is harvesting and storing abundant energy, such as solar energy. Photovoltaic cells are particularly suitable here, by transferring solar energy directly to electrical energy. While solar cells based on silicon or metal-organic perovskites are very popular and often investigated [1–8], the full oxide counterpart is much less known [9]. Solid oxide based solar cells have been realized using for example metal/Cu_2O Schottky junctions [10–14], Cu_2O/ZnO bilayer heterojunctions [15–17], nanocomposite heterojunctions with nano-structured ZnO or TiO_2 on Cu_2O [18–22], and also $BiFeO_3$ domain boundaries [23,24], all operating at room temperature.

Also, many other oxides show interesting properties when irradiated by UV light, such as Nb_2O_5 [25,26], SnO_2 [27–30], and $SrTiO_3$ (STO) [31–36]. Among others, it was shown for STO that the uptake of oxygen at elevated temperatures is tremendously enhanced by UV light [37,38]. Moreover, it is reported that voltages resulting from STO based cells under UV light may consist of a photovoltaic (PV) and an electrochemical contribution (EC), the latter being the result of a change in oxygen stoichiometry in STO due to the enhanced oxygen incorporation under UV irradiation [39]. STO based heterojunctions, e.g. the STO/Si interface, generate photovoltages at room temperature with a very fast response [40,41]. Also, Nb:STO based pn-junctions or Schottky junctions [42–54] have been investigated as photovoltaic devices, mostly operating at room temperature. Recently, it was found that the (La,Sr)CrO_3 (LSCr)/STO junction can be used to obtain photovoltages up to 1 V at temperatures above 300 °C [55]. Coupling such a high temperature solar cell with a solid oxide electrolyzer cell (SOEC) yields a photoelectrochemical cell (SOPEC) which can pump oxygen and may ultimately even use UV light to split water, thereby transferring solar energy to electrical energy and further to chemical energy [55]. Such devices benefit from the lower resistance of oxides at higher temperatures and might be used for small scale energy harvesting applications, e.g. for powering sensors for the internet of things, in surroundings where heat is abundant.

* Corresponding author.
E-mail address: alexander.e164.schmid@tuwien.ac.at (A. Schmid).

https://doi.org/10.1016/j.ssi.2021.115700
Received 18 March 2021; Received in revised form 22 June 2021; Accepted 23 June 2021
Available online 13 July 2021

This type of high temperature STO based solar cells are in the focus of our study. Here, we show why the illuminated surface of such solar cells is crucial and how photovoltages change with different top layer materials. The dopant level of Sr was varied in $La_{1-x}Sr_xCrO_3$ ($LaCrO_3$ (LCr), $La_{0.9}Sr_{0.1}CrO_3$ (LSCr10) and $La_{0.8}Sr_{0.2}CrO_3$ (LSCr20)) and Cr was replaced by Mn on the B-site of the perovskite, yielding $La_{0.8}Sr_{0.2}Cr_{1-y}Mn_yO_3$ (LSCrM). Other perovskite type oxides, including $La_{0.6}Sr_{0.4}FeO_3$ (LSF) and $La_{0.6}Sr_{0.4}CoO_3$ (LSC) and Pt and Au were tested as metallic top layers. Moreover, we investigated self-enhancement effects under operation and the influence of the STO substrate, with Fe:STO showing slower changes than undoped STO, highlighting the very importance of the STO substrate itself for the overall function of such cells. Further mechanistic insight into the processes under UV is gained by impedance spectroscopic measurements. Essentially, we show that (classical) Schottky junctions can be used for high temperature photovoltaic devices, allowing possible high temperature applications (e.g. space applications, concentrated sunlight, combined cells with solid oxide electrolyzer cells…). However, classical systems fail to function in such high temperature conditions.

2. Experimental

2.1. Sample preparation and characterization

The solar cell consists of a single crystalline substrate, namely (100) oriented undoped STO ($10 \times 10 \times 0.5$ mm^3, CrysTec GmbH, Ger) or Fe:STO ($10 \times 10 \times 0.5$ mm^3, 0.016 mol% Fe, Alineason Materials Technology GmbH, Ger) and a thin top layer of another oxide or a metal. All sample types are summarized in Table 1. The oxide top layers (e.g. LSCr) were deposited by pulsed laser deposition (PLD) using a Kr/F excimer laser Lambda COMPex Pro 201F with a wavelength 248 nm. The repetition rate was 5 Hz with a nominal energy per pulse of 400 mJ, yielding a laser fluence of 1.1 J/cm^2. The LSCr and LSCrM thin films were deposited at 700 °C and 0.015 mbar and the deposition time was varied. As a current collector, Pt stripes were deposited by DC magnetron sputtering (BAL-TEC MED 020 Coating System; pressure: 2×10^{-2} mbar Ar, 100 mA) on top of the oxide thin film. The structuring of the Pt thin film was carried out by lift-off photolithography. The width of the Pt stripes is 100 μm, with a distance of 50 μm between the individual Pt stripes, corresponding to an area fraction of two thirds being covered with Pt. At the bottom side of the sample, a porous Pt paste was brushed as a counter electrode. A schematic representation of the sample is given in Fig. 1a. Metal (Au, Pt) top layers with thicknesses mostly of about 10 nm were sputter deposited in the same way as the current collectors mentioned above. A quartz microbalance was used to determine the deposition rate of Au and Pt.

Table 1
Thickness of the ceramic or metallic thin films on STO substrates.

Top layer	Substrate	Preparation method	Deposition time [min]	Thickness [nm]
$LaCrO_3$ (LCr)	$SrTiO_3$ (STO)	PLD	25	180
$La_{0.9}Sr_{0.1}CrO_3$ (LSCr10)	$SrTiO_3$ (STO)	PLD	5	50
$La_{0.9}Sr_{0.1}CrO_3$ (LSCr10)	$SrTiO_3$ (STO)	PLD	25	240
$La_{0.9}Sr_{0.1}CrO_3$ (LSCr10)	Fe:$SrTiO_3$ (Fe:STO)	PLD	25	240
$La_{0.8}Sr_{0.2}CrO_3$ (LSCr20)	$SrTiO_3$ (STO)	PLD	25	230
$La_{0.9}Sr_{0.1}Cr_{0.8}Mn_{0.2}O_3$ (LSCrM)	$SrTiO_3$ (STO)	PLD	25	240
$La_{0.9}Sr_{0.1}Cr_{0.2}Mn_{0.8}O_3$ (LSCrM)	$SrTiO_3$ (STO)	PLD	25	240
$La_{0.8}Sr_{0.2}MnO_3$ (LSM)	$SrTiO_3$ (STO)	PLD	3	50
$La_{0.8}Sr_{0.2}MnO_3$ (LSM)	$SrTiO_3$ (STO)	PLD	25	400
Au	$SrTiO_3$ (STO)	sputtering	0.16	10
Au	$SrTiO_3$ (STO)	sputtering	3.3	200
Pt	$SrTiO_3$ (STO)	sputtering	0.26	10

The oxide thin films on STO were characterized by X-ray diffraction (XRD) and cross-section scanning electron microscope (SEM) imaging. Fig. 2 displays the diffraction pattern of an LSCr10 film on STO measured with a goniometric scan between the 2-theta angle of 10° and 99°, using Cu $K_{\alpha 1}$ radiation. Only the (100), (200) and (300) reflexes are visible. In the magnifications of the (100) and (300) reflexes, one can see the sharp reflexes of the STO single crystal (i.e. the substrate) and the broader thin film reflex of the LSCr10 layer. With only the (h00) reflexes being visible, this suggests that the LSCr thin films grow epitaxially on the $SrTiO_3$ substrates. However, nominally the LSCr10 reflexes are expected at higher angles than the respective (h00) reflexes of STO. The shift towards lower angles is attributed to defects in the thin film, most likely cation vacancies which are frequently found in different complex oxide thin films prepared by pulsed laser deposition [56,57]. The thickness of the ceramic thin films was determined by profilometry as well as SEM cross sections (see Fig. 2b). A cross section of the interface between LSCr10 and STO is shown in Fig. 2b. Please note that despite the focus on thin film characterization the "powerhorse" of such a cells in terms of charge carrier formation is the illuminated region of the STO substrate as well as the space charge region, i.e. the interplay of thin film and substrate, in terms of charge carrier separation.

2.2. Photo-voltage and photo-current measurements

For photo-voltage and photo-current measurements, the sample was placed in a quartz tube inside a furnace. A quartz waveguide (10 mm in diameter) leads the UV light ($\lambda = 365$ nm, $P = 2.9$ W) from the LED lamp (LZ4 LuxiGen UV LED Emitter, LED Engin, USA) outside the furnace to the sample, as shown in Fig. 1b and c. A Keithley DMM2000 (Keithley Instruments, USA) was used for voltage and current measurements. The resulting voltage was measured mostly in open circuit mode (OCV = open circuit voltage) and the current in short circuit. All measurements were performed at 350 °C in air. The standard procedure for OCV measurements was the following: The voltage was measured for 15 min without UV irradiation, followed by 15 min under UV light and then again for 15 min after switching off the light. Thereby, the dark voltage before the experiment, the time dependent evolution of a photovoltage and the persistent [58–60] or decaying photovoltage after illumination can be observed. Short circuit measurements were done in a similar manner, though partly longer illumination times were used or the current measurement was interrupted for an OCV measurement upon UV. Moreover, time dependent power-voltage and power-current curves were obtained for illuminated cells.

2.3. Spectroscopic ellipsometry measurements

Spectroscopic ellipsometry (SE) measurements were carried out in a Horiba iHR320 monochromators UVISEL ellipsometry system, with spectral range 0.6–5.0 eV and step size 0.05 eV. The spectra were collected with a light incidence angle of 70° and with the modulator and analyzer set at 0° and 45°, respectively. In order to measure the oxide films, sample replicas of the materials in Table 1. Were prepared, i.e. $LaCrO_3$, $La_{0.8}Sr_{0.2}CrO_3$, $La_{0.9}Sr_{0.1}Cr_{0.2}Mn_{0.8}O_3$ and $La_{0.8}Sr_{0.2}MnO_3$, on top of an Al_2O_3 (0001) substrate. Modelling of the optical response was carried using DeltaPsi2 software by Horiba. The model followed a geometry in which the material layer is placed on top of a well-defined Al_2O_3 substrate. The thickness of the layers was fixed in agreement with the SEM characterization. A 1 nm material-void (50% each) overlayer was fixed on top of the material layer in order to simulate the contribution of the film roughness. The material was then fitted with a

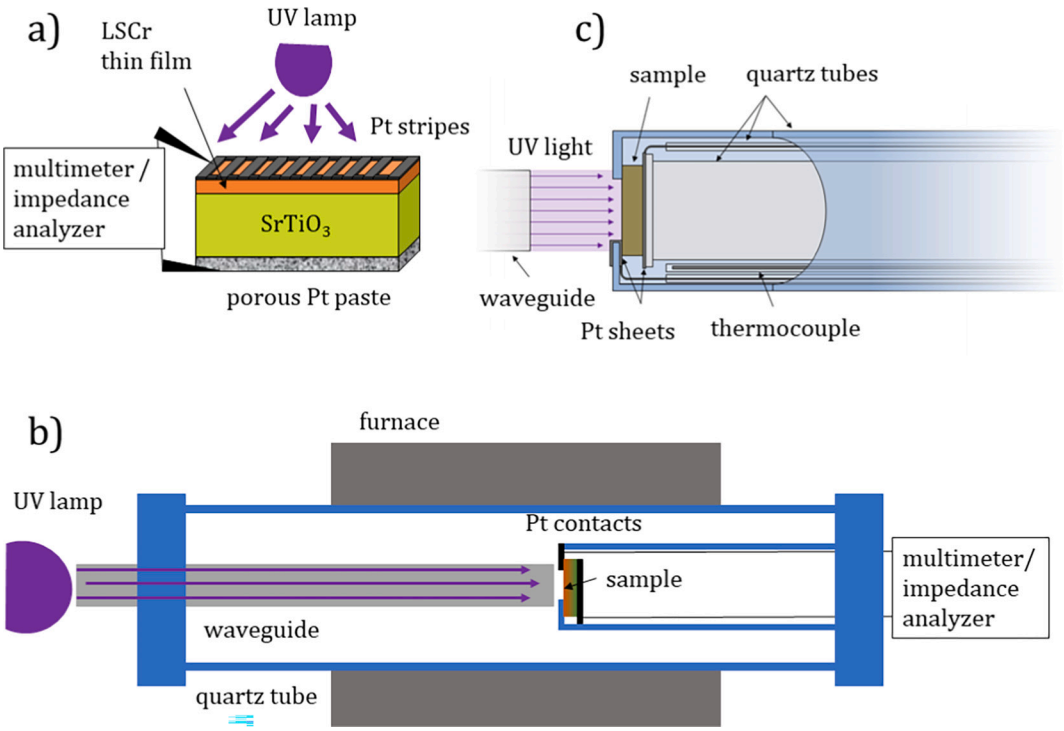

Fig. 1. Typical sample consisting of an STO substrate and an LSCr thin film (a), the measurement setup consisting of a quartz tube in a furnace, a waveguide with a LED lamp and a sample holder with contacts for electrochemical measurements (b), and a detailed view on the sample holder (c).

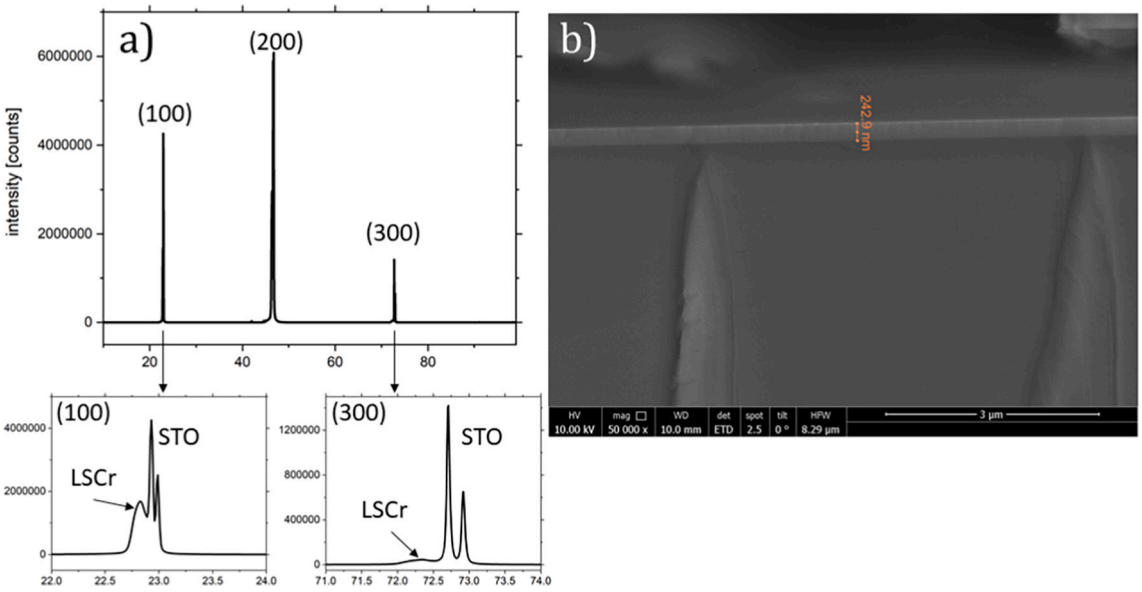

Fig. 2. Thin film characterization. X-ray diffraction pattern of LSCr10 on STO, showing very good agreement between the LSCr reflexes and the single crystalline STO reflexes of the substrate, therefore highlighting the epitaxial nature of the LSCr/STO interface (a). SEM image of the interface showing the LSCr10 thin film on top of the STO substrate (b).

series of 5xTauc-Lorentz (TL) user-defined-formula (udf) dispersion oscillators. The use of TL oscillators has been widely reported to fit the dielectric properties of semiconductor perovskites [61–63]. As a result, one can obtain data on the layers´ optical constants.

For analyzing the optical properties of STO, an STO single crystal substrate was kept in the PLD chamber at the deposition conditions of the oxide films (i.e. 25 min of deposition time) before measuring the optical properties. Thus, the measurement is consistent with the nature of the STO present in the photovoltaic device. The model chosen for STO was quite similar to the case of the films, with the roughness overlayer directly placed on top of the substrate material. For properly fitting the STO optical properties, a series of 4xTL oscillators were required. The general expression of light absorption in a solid $I=I_0e^{-\alpha t}$, where I is the is the transmitted light, I_0 is the incident light, α is the absorption coefficient of the solid and t is the thickness was used to calculate the percentage of adsorbed light at a given wavelength.

2.4. Electrochemical impedance spectroscopy measurements

Electrochemical impedance spectroscopy was performed using an Alpha-A High Resolution Dielectric Analyzer (Novocontrol, Germany) in frequency range from 1 MHz to 1 Hz with a resolution of 10 points per decade and an rms amplitude of 20 mV. In special cases, the frequency range was extended down to 31 mHz. Impedance spectra were measured under short circuit conditions (bias 0 V). The obtained impedance data were parameterized by equivalent circuits using ZView3.5 (Scribner, USA).

3. Results and discussion

3.1. Photo-voltages

Fig. 3a displays the results of a standard OCV experiment on a sample with a 240 nm LSCr10 top layer (15 min dark, 15 under UV, 15 min dark). A schematic representation of the band alignment between the respective materials is sketched in Fig. 3b, showing the difference in Fermi energy which leads to the photovoltage under UV. Upon UV light, an immediate voltage step to almost 730 mV is found in Fig. 3a, followed by a further increase within about 100 s to a nearly constant value of ca. 930 mV. Here, we expect a polarity of – for LSCr and of + for STO. After switching off the UV light, the voltage is reduced but does not immediately jump to zero. Rather, the decay to zero voltage requires several 10 s or even a few minutes. Generally, the time with a transient change of the voltage was longer after switching off UV compared to switching UV on. The same phenomenon is also found for Fe-doped STO as substrate (Fig. 3), however, the increase of the photovoltage under UV takes even much longer in this case. These time dependencies are most probably caused by changes of the oxygen stoichiometry in STO upon UV light [37–39] and subsequent relaxation to the equilibrium defect concentrations in dark. This is discussed in more detail below.

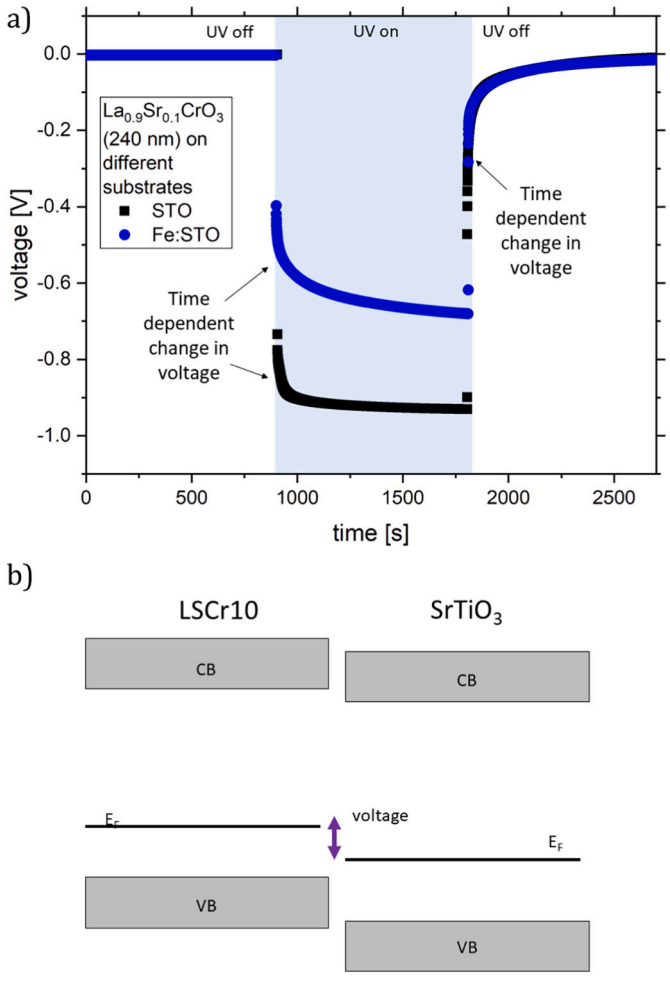

Fig. 3. (a) Time vs. voltage curves for LSCr10 (−)/STO (+) and LSCr10 (−)/Fe:STO (+) samples at 350 °C in air, with the signs in brackets indicating the polarity of the respective part of the cell. At first, the voltage is measured for 15 min without UV light, then for 15 min under UV illumination (λ = 365 nm), then for 15 min after switching off the UV light. When switching on the UV light, a time dependent change in voltage can be observed for both substrates, but the change occurs at a different speed. When switching off the UV light, a voltage of several hundred mV remains. Here, the time dependency of the decaying voltage appears to be similar for both cases. (b) Sketch of the band alignment of LSCr10 and STO with the conduction bands (CB) and valence bands (VB) of the respective materials. The difference in Fermi levels is highlighted.

Qualitatively, the same features are found for many different oxide top layers. A representative collection of layer variations is shown in Fig. 4. In Fig. 4a the Sr dopant concentration of $LaCrO_3$ was varied between 0 and 20%. For higher Sr concentration, the total conductivity of the LSCr layer rises [64], but the thin film also changes in color, from a nearly transparent undoped LCr thin films to the light brownish LSCr20. The highest voltage results for undoped $LaCrO_3$ (LCr) (1008 mV). The cell with LCr top layer also exhibits the slowest voltage relaxation after switching UV off, possibly due to the slow oxygen exchange between LCr and the gas phase, which is required to get the STO back to its equilibrium defect chemical state after UV.

When replacing Cr by Mn while keeping the deposition time constant (i.e. similar layer thickness), we find a decrease of the photo-voltage (Fig. 4b). Fig. 4c displays effects of the film thickness for LSCr10 and LSM top layers. For LSCr10 thin films, the resulting OCV is very similar for different layer thicknesses, with 930 mV for 240 nm and 990 mV for 50 nm. In case of LSM, however, the thin layer with 50 nm achieved 910 mV while the thicker one with 400 nm only reached 610 mV. Most probably, this is largely due to the much higher UV absorbance of LSM, which makes it much darker than LSCr10 for similar layer thickness. Accordingly, much less light reaches the heterojunction between top layer and STO.

These results also strongly suggest that UV absorption within STO is essential for the generation of the photovoltage, i.e. STO acts as the absorber of our high temperature oxide solar cell.

Also, LSF and LSC perovskite-type top layers were tested. These thin films have an intense black color and thus high absorption. Not surprisingly, only low photovoltages were obtained (e.g. 40 mV for LSF of 100 nm thickness). These findings are in line with the results on LSCr, highlighting the importance of a high transmittance in the top layer. However, possibly the different electronic band structure and/or the ionic defect energies in LSC or LSF contribute to the much lower photovoltages as well.

Very thin metal layers (10 nm Au, 10 nm Pt) with some remaining UV transmittance [65] were also investigated as top layers. The results are plotted in Fig. 4d. The photovoltages obtained for Pt were only mediocre (400 mV range) but for the very thin Au layer we found 1100 mV at 350 °C and thus the highest value of all layers tested in this study. All these measurements also demonstrate the “robustness” of the PV voltage of STO based high temperature solar cells; it is not a peculiarity of a very special materials combination, but results for many different materials. For the photovoltaic effect upon UV light, the STO single crystal is vital, meaning that the relevant processes are located within the STO. The role of the top layer is most likely primarily the introduction of chemical potential differences for electrons (and possibly also for oxygen vacancies) at the interface and thus the formation of a space charge region in STO. This space charge layer in the slightly hole conducting STO acts as barrier for the holes (majority carriers) while attracting photo-generated electrons in STO and swamping them into the top layer. Therefore, many thin films with acceptably low absorption cause photovoltages upon illumination. The space charge region is

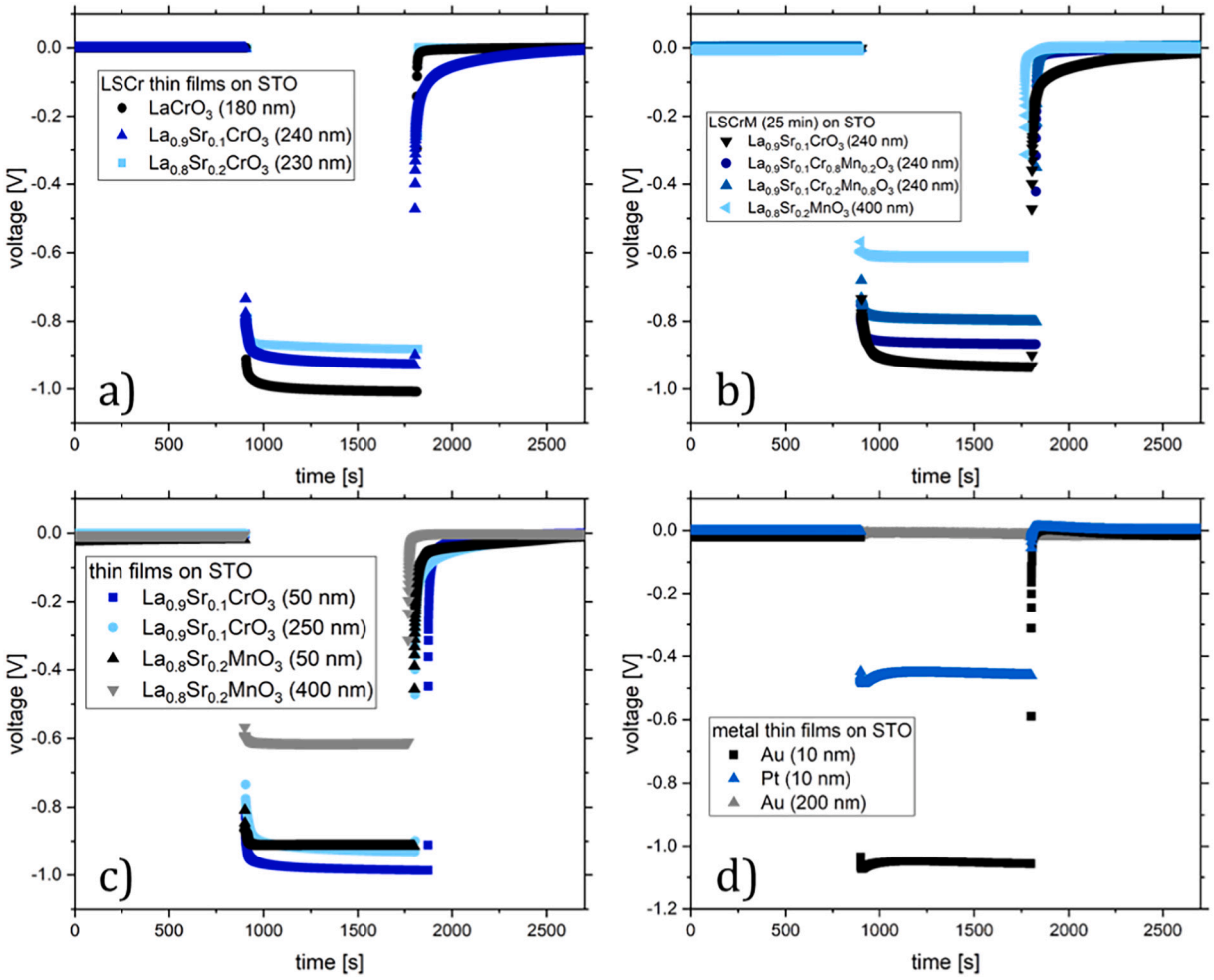

Fig. 4. Voltage-time curves at 350 °C in air for different material combinations before, under and after UV illumination (λ = 365 nm), showing the influence of (a) different Sr dopant concentrations in LSCr, (b) the introduction of Mn to the B site of the LSCr, (c) the thickness of LSCr10 as well as LSM thin films, and (d) metallic thin films.

visible as a very large additional resistance (second semicircle) in impedance spectra and its dependence on UV light is discussed in more detail below. The recombination length of the electrons in our STO single crystals is unknown and hence we do not know from which depth photo-generated electrons can be collected and contribute to the operation of the solar cell. The upper limit is certainly the absorption depth of UV in STO.

This interpretation is also supported by optical SE measurements. The absorption of both oxide thin films (top layers) and STO substrate was investigated. The resulting absorption spectra are shown in Fig. 5a. From here, considering a 365 nm UV light source (3.4 eV), the percentage of absorbed light as a function of the material's thickness was calculated (Fig. 5b). Please note that the obtained spectra are in line with previous reports [63,66–68]. It should be noticed, however, that slight deviations may arise [69,70], possibly due to differences in the synthesis method or as a consequence of the technique used for the measurement.

The relevant optical properties are summarized in Table 2 which also includes the absorption depth of the films, i.e. the thickness within which 95% of the light is absorbed. The relation between absorbed light in such a layer and the photo-voltage is shown in Fig. 5c. For layers with very strong absorption the photo-voltage decreases. (The intensities used here are rather high and thus already less than 20% transmitted light leads to very high photo-voltages.) However, a slight difference between Mn and Cr based perovskite top layers seems to remain irrespective of transmittance, since the thin LSM layer with much more transmittance has still a slightly lower OCV than LCr. As far as the STO substrate is concerned, an estimation of 2 μm for the absorption depth was obtained.

3.2. Photocurrent under UV

For photovoltaic cells, current voltage curves are frequently reported. However, as will be shown in the following, the current of our STO based PV cells is strongly time dependent and current measurements are most probably accompanied by continuous oxygen stoichiometry changes within the STO single crystals. Accordingly, the cells change continuously during current load and steady state current voltage curves could not be determined. Hence, we focus the following consideration on the short circuit current as the most extreme case of a current flow. This was investigated for an LSCr10/STO cell with 240 nm LSCr10. When switching on the UV light for the very first time, a rather low current in the 2–5 μA range results (see magnification in Fig. 6a). However, over time this current strongly increases by orders of magnitude. After 15 min 0.18 mA are reached but the current is still far from being constant (Fig. 6a). Long-term measurements in Fig. 6b show that the current increase becomes slower, but persists on the time scale of many hours. The almost linear long time current increase reaches almost 1 mA after 17 h. Some samples even showed photocurrents of up to 3.5 mA at 350 °C after several illumination cycles, all for a nominal sample size of 1 cm^2.

This current increase is not accompanied by a decrease of the OCV, as

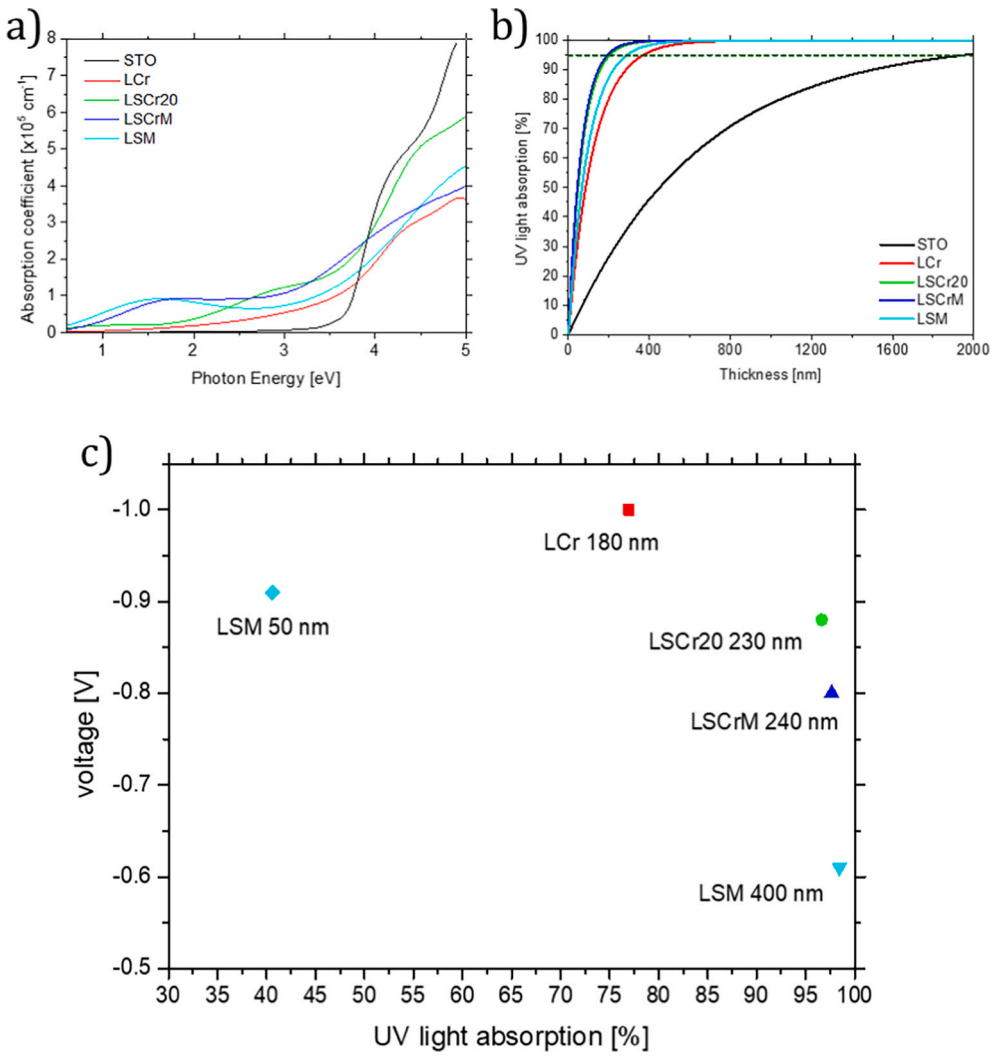

Fig. 5. Absorption spectra for the different materials under consideration (a). Percentage of UV light absorbed (365 nm) as a function of material's thickness. The horizontal dotted line indicates the thickness at which 95% of UV light is absorbed (absorption depth) (b). Measured PV vs percentage of light absorbed for different top layers (c).

Table 2
Absorption measurements.

Layer	Absorption coefficient at 365 nm [cm^{-1}]	Absorption depth [nm]	Percentage light absorbed [%]
$LaCrO_3$ (LCr)	81,522	367	76.9
$La_{0.8}Sr_{0.2}CrO_3$ (LSCr20)	147,603	203	96.6
$La_{0.9}Sr_{0.1}Cr_{0.2}Mn_{0.8}O_3$ (LSCrM)	156,700	191	97.7
$La_{0.8}Sr_{0.2}MnO_3$ (LSM)	104,185	288	40.6 (50 nm) 98.5 (400 nm)
$SrTiO_3$ (STO) single crystal	15,405	1945	–

The percentage of UV light absorbed was calculated considering the layers' thickness as retrieved by SEM cross-section data.

shown in Fig. 6c: There, 5 min of OCV measurement under UV (reaching 1050 mV) are followed by a short circuit period of 5 min with a strong current increase to the several 100 μA range. Please note that here the sample was already illuminated in a preceding experiment. The initial short circuit current under UV is thus much larger than for the pristine sample, indicating that the sample changes caused by the preceding illumination are still (partly) present. However, despite all these changes, the subsequent OCV measurements show again more than 1 V, indicating that the cell voltage itself is hardly affected by the persisting sample changes upon current. In other words, the cell's power shows a very pronounced enhancement effect during operation. This becomes also visible in continuous P versus voltage V measurements (and the power P versus current I curves) monitored on an LSCr10/STO sample, see Fig. 7. A severe enhancement is found already within several minutes. (Please note that sample changes take place also within a single P (V) curve which takes 10 s). The difference in time scales for time dependent photovoltage changes (in the range of few minutes) and photocurrent measurements (in the range of several hours) is addressed in Section 3.4.

We suppose that the origin of these changes upon current lies within the very nature of the measurement itself. As soon as current flows, there is a voltage drop not only at the external load but also inside the PV cell at the internal resistance. In the specific case of short circuit even the entire photovoltage of more than 1 V is "consumed" in the sample itself. STO is a mixed electronic and ionic conducting material and the ions are strongly blocked at one or both electrodes used here. Applying a voltage of about 1 V to such a STO sample leads to oxygen stoichiometry polarization, i.e. oxygen vacancy depletion in the STO bulk close to the positive electrode and their accumulation close to the negative one [71–73]. Often this is associated with a resistance degradation, since

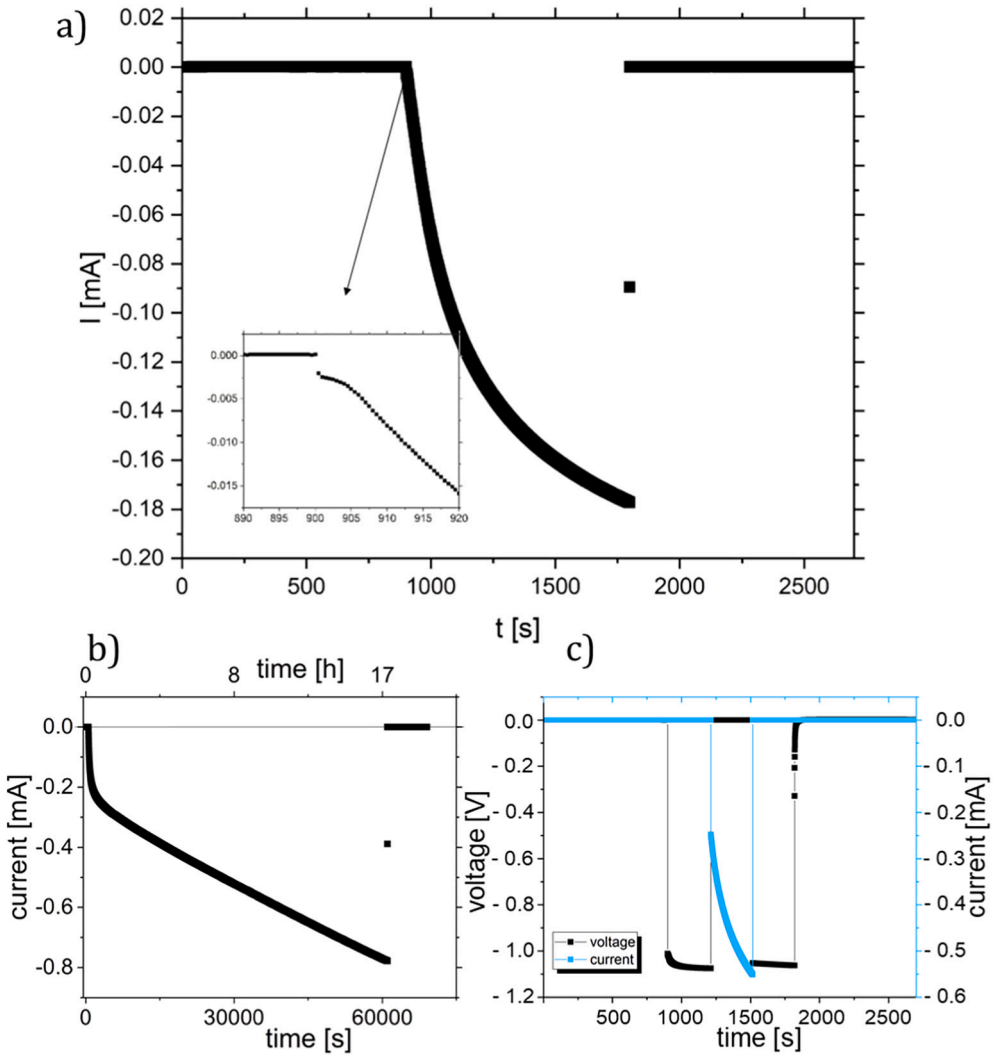

Fig. 6. Current-time measurements for LSCr10 (250 nm thickness) on STO at 350 °C in air (1 point/0.5 s). The measurements show a steady current increase under UV light (λ = 365 nm) on a short time scale (a) but also a continuous increase even after 17 h under UV light (b). Consecutive voltage, current and voltage measurements indicate only a small effect of the changes under current on the photovoltage (c).

also reorganization of electrons and holes takes place for the sake of charge neutrality [74,75]. Higher conductive regions are formed near to the electrodes and then extend more and more into the bulk. Hence, a steady decrease of the cell resistance results.

We expect the same taking place here, though the voltage is not applied by an external source, but is a consequence of the UV illumination. This effect has two implications: Firstly, measuring a well-defined current-voltage curve or a power-voltage curve is not truly possible for these STO based systems, since the cell unavoidably changes during the measurement. Secondly, one can benefit from this self-enhancing effect due to a decrease in STO resistance, leading to a better performance under operation ("self-enhancing solar cell").

3.3. Electrochemical impedance spectroscopy

Electrochemical impedance spectroscopy (EIS) was performed on LSCr10/STO heterojunctions at 350 °C without correction of the open circuit voltage, i.e. under short circuit conditions (U = 0 V). Therefore, these measurements give mechanistic insight into the processes found for the current measurements discussed above. The impedance spectrum of the solar cell before illumination is shown in Fig. 8a. The three main features are a high frequency semicircle, a mid frequency arc and a very large low frequency arc. The high frequency semicircle (r.h.s inset in Fig. 8a) reflects the bulk resistance and capacitance of the STO single crystal, with a relative permittivity of 170 calculated from the corresponding capacitance, in accordance with bulk STO at 350 °C [76]. The low frequency feature is attributed to the space charge region (SCR) at the STO/LSCr10 interface [55] and represents the photoactive part of the cell, which ultimately separates the photo-generated electron-hole pairs in STO. Some further details on this space charge impedance can be found in Ref. [55]. Actually, it is nothing but a Schottky barrier found very often between semiconductor/electrode interfaces. In accordance with Ref. [55] the intermediate frequency feature is attributed to the bottom electrode of the PV cell.

The time dependent changes in the impedance spectra under and after UV light illumination are shown in Fig. 8b–d. The first spectrum measured immediately after switching on UV is completely distorted due to the ongoing changes upon UV and can hardly be analyzed. The second spectrum is started 3 min after onset of UV illumination and indicates a strong decrease of the high frequency arc, which is now only partly visible in this measured frequency range. The low frequency part with spiral-type tail indicates that the sample still changes while being measured with frequencies sweeping from high to low values. In the third spectrum (started after 15 min) the STO bulk resistance is only visible as an axis intercept and has a value which is two orders of magnitude smaller than before UV. The remaining low frequency arc

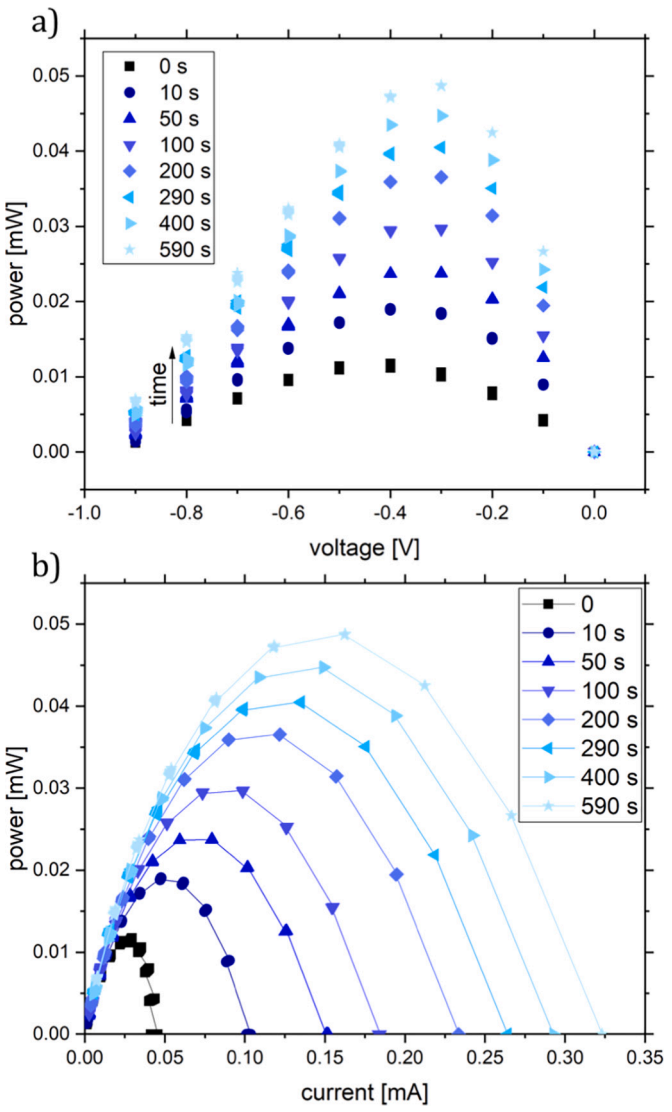

Fig. 7. Power-voltage (a) and power-current (b) curve of a UV illuminated LSCr10/STO cell at 350 °C in air (λ = 365 nm), highlighting the self-enhancing character of the solar cell. One measurement point requires 1 s (i.e. 10 s for one P(V) or P(I) curve); sample size 1 cm^2.

might be the remains of the photo-active top space charge layer under UV or the impedance of the bottom electrode/electrolyte contact. (Please note that even without being illuminated itself the bottom layer space charge might change under illumination due to our supposed stoichiometry variation in the STO bulk.) When switching off UV the huge top layer space charge is back already in the very first spectrum (Fig. 8c), while the high frequency arc of bulk STO only slowly relaxes and increases from spectrum to spectrum. After about 50 min the original value is again reached.

From this we conclude that indeed the conductivity and thus also the defect chemical state of the STO bulk changes upon UV under short circuit conditions. As detailed above, this change is most probably nothing but the well-known stoichiometry polarization often found in STO samples upon a voltage, when one or both electrodes are strongly blocking for ionic current, i.e. electrochemical oxygen exchange. In order to support the consistency of this interpretation, we further looked at the time dependence of the large space charge resistance under and after UV. Since recording an entire impedance spectrum takes several minutes, the time resolution was not sufficiently high to follow this very fast process. Therefore, impedance was measured continuously at 1 Hz (see Fig. 9). This impedance value is in the left half of the space charge arc measured in dark. The location of this frequency within the corresponding arc changes under illumination. However, we also know the shape of the impedance spectra before, under and after UV light illumination (Fig. 8), which makes analysis straightforward. We see that the impedance at 1 Hz and thus the entire space charge arc changes immediately (i.e. within <1 s) and drastically when illuminating by UV light. This is in line with the immediate changes found in current measurements in Fig. 4. This immediate change under UV light is followed by a steady further decrease in the resistance, which reflects the self-improvement of the cell discussed above. When switching back to dark the huge space charge arc appears again within the first second and the subsequently following slight shift in Fig. 9 might be simply due to the change of the STO bulk itself, which is much slower.

3.4. Interpretation of the OCV measurements

One characteristic feature of these cells has still to be interpreted: It is the time dependence of the cell voltage under OCV conditions (see Fig. 3). The space charge relaxes within a second when UV light is switched off (see above) and thus zero voltage is expected immediately when stopping illumination. Stoichiometry changes upon current flow (as in the short circuit case) can also not explain these finding since no current flows under OCV. However, we are confident that stoichiometry changes in STO upon UV still play a decisive role as discussed in the following. Our explanations are based on interpretations of UV induced effects in STO single crystals reported in Ref. [37–39].

In Ref. [37], a strong enhancement of the oxygen incorporation rate into Fe-doped STO was found under UV illumination. Moreover, in Ref. [38], it was shown that substantial conductivity changes result during and after illumination of such STO single crystals. Importantly, these conductivity changes also affect the dark parts of the STO beyond the absorption depth. They are associated with stoichiometry changes due to UV-accelerated oxygen incorporation. Essentially, the hole conductivity of the entire STO sample strongly increases under illumination due to oxygen vacancies being annihilated under UV in the entire bulk. The corresponding time dependence of the conductivity changes upon UV is governed by the chemical diffusion coefficient of oxygen in STO. This chemical diffusion is slower for Fe-doped STO compared to undoped STO due to the trapping of hole charge carriers [77]. In other words: the oxygen chemical potential of an illuminated STO samples changes under UV due to oxygen incorporation and when switching off UV, a very high chemical potential (nominal by high oxygen partial pressure) remains in the sample. This can be measured in terms of a positive voltage, particularly when covering the bottom side of STO with an ion conducting yttria stabilized zirconia (YSZ) layer and thus making STO to a kind of electrode in an electrochemical cell [39]. The measured voltage is nothing but a Nernst-type voltage between the STO (no longer in equilibrium with the gas) and the YSZ covered bottom side. This is sketched in Fig. 10a, together with the typical voltage curve found in such cells [39] with a mixture of fast photo-effect and slower stoichiometry effects. Most important is the remaining voltage after UV (U_{bat}) which is due to the chemical potential change in STO under UV and only slowly relaxes at ca 350 °C.

Compared to the cell in Ref [39], the top side is continuously covered in our solar cell, e.g. by LSCr, and the ion conducting bottom YSZ layer is missing (see Fig. 10b). As in the cell with the free STO surface, similar time dependencies are found, but first the voltage further increases upon UV and second the remaining voltage after UV is negative in our case. The following explanation of these phenomena is still hypothetical, but consistent with all data we have so far: The chemical potential of oxygen μ_O is given by the difference of the chemical potentials of ionic and electronic species (V_O = oxygen vacancies, e = electrons, h = holes):

$$\mu_O = \mu_{O^{2-}} - 2\mu_e = -\mu_{V_O} + 2\mu_h. \quad (1)$$

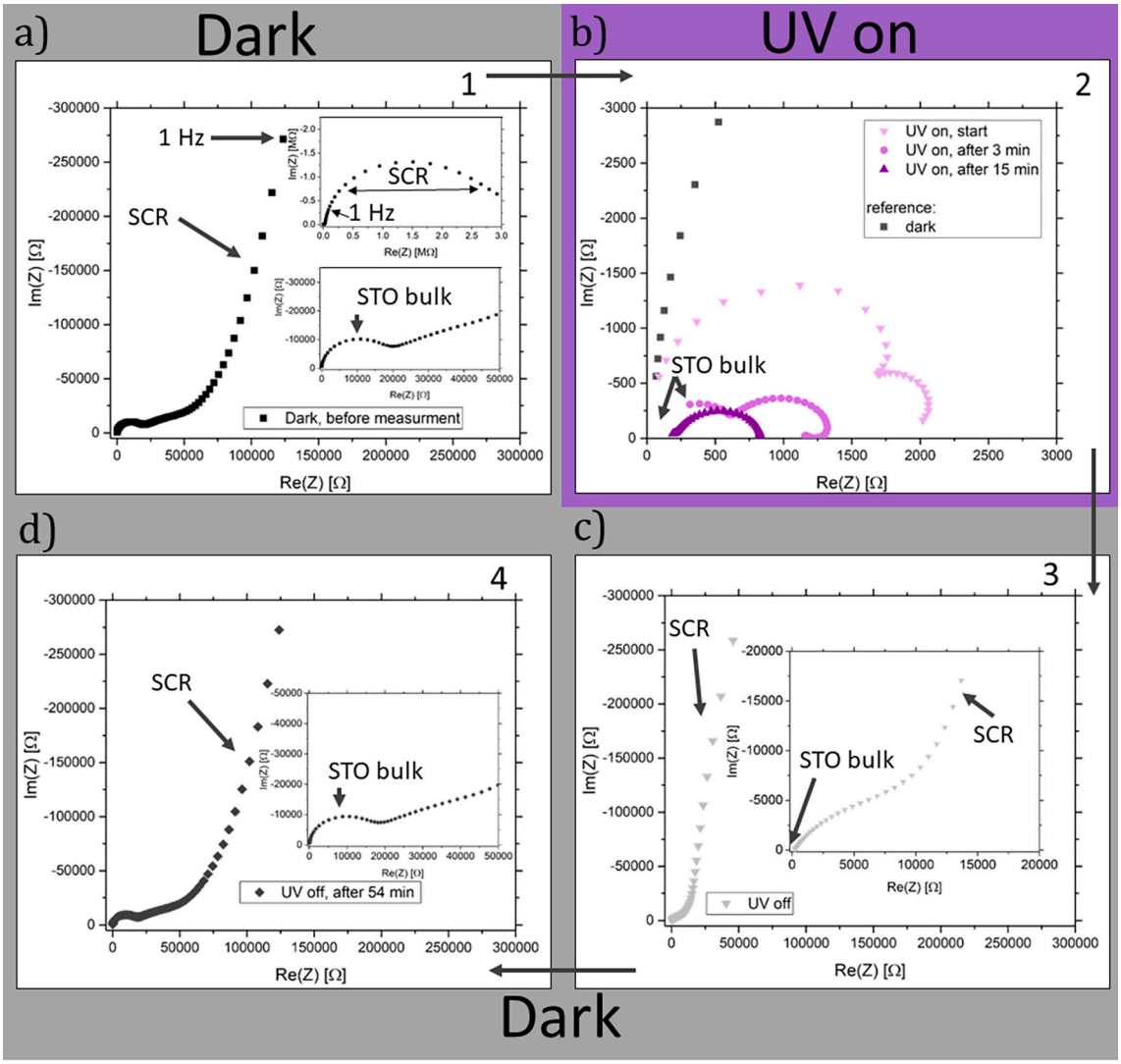

Fig. 8. Impedance spectra of LSCr10/STO samples at 350 °C in air in darkness and under UV light (λ = 365 nm) with: (a) Impedance spectrum of a LSCr10/STO solar cell without UV illumination ("dark"). The three main features are the high, mid and low frequency semicircle. The high frequency semicircle (ω_p approx. 80 kHz) is attributed to the bulk STO. The low frequency semicircle (ω_p approx. 0.080 Hz) originates from the space charge region (SCR) at the LSCr/STO interface. The mid frequency feature most likely comes from the bottom electrode. (b) Time dependent evolution of impedance spectra during UV light illumination and (c,d) after UV. The contributions of STO bulk resistance (STO) as well as the resistance of the space charge region (SCR) are identified in the individual impedance spectra. Under UV light, two processes take place: i) The very fast vanishing of the space charge resistance; ii) the continuous drop in STO resistance upon switching on the UV light due to stoichiometry polarization.

In contrast to cell type a in Fig. 10 (with free illuminated STO surfaces), UV light does not directly accelerate oxygen incorporation kinetics into STO since the surface of cell b is covered by LSCr. However, in the illuminated part of STO (≈ 2–3 μm deep as resulting from SE measurements) the UV light causes a split of μ_e into two quasi Fermi levels (one for electrons and one for holes). Therefore, also two quasi chemical potentials of formally neutral oxygen result in accordance with Eq. (1). Owing to a spatially varying absorbance, those quasi chemical potentials show gradients and cause oxygen diffusion within STO. Depending on the local concentrations of holes and electrons, the illuminated STO region gets either enriched or depleted of oxygen vacancies. Supposed we pump some oxygen from the illuminated region into the dark part (by chemical diffusion of vacancies and holes), a situation results where the illuminated part has a different defect chemical state and thus also a different (quasi-)Fermi level compared to the initial situation under UV. Not surprisingly the open circuit voltage changes during this oxygen relocation inside STO and this is what supposedly causes the time dependence of the OCV voltage under UV. In Fe-doped STO the change is simply slower since it has a smaller oxygen diffusion coefficient due to its Fe-traps [77]. A simple estimate of a diffusion distance from the measured time of voltage variation (ca. 1000 s for Fe-STO) and the oxygen diffusion coefficient D in Fe-STO at this temperature (10^{-8} cm^2/s [78,79]) gives 3 μm, which is well in line with the illuminated STO depth according to SE.

When switching off UV, all PV effects are gone but the formerly illuminated layer is still enriched in oxygen vacancies and has a lower chemical potential of oxygen compared to the rest of the STO. This causes a Nernstian cell voltage with an opposite sign compared to the cell in Fig. 10a (Here the required ion conductor is no longer YSZ, but the STO zone with oxygen vacancies.) The oxygen chemical potential finally relaxes by diffusion inside STO but also by some oxygen incorporation across the top layer and rather quickly decays. Supposed the oxygen incorporation via the top layer is the decisive process during this relaxation, also the same time dependence for Fe-STO and STO can be explained. We are well aware that despite explaining our findings, the given model is not sufficiently backed by independent measurements

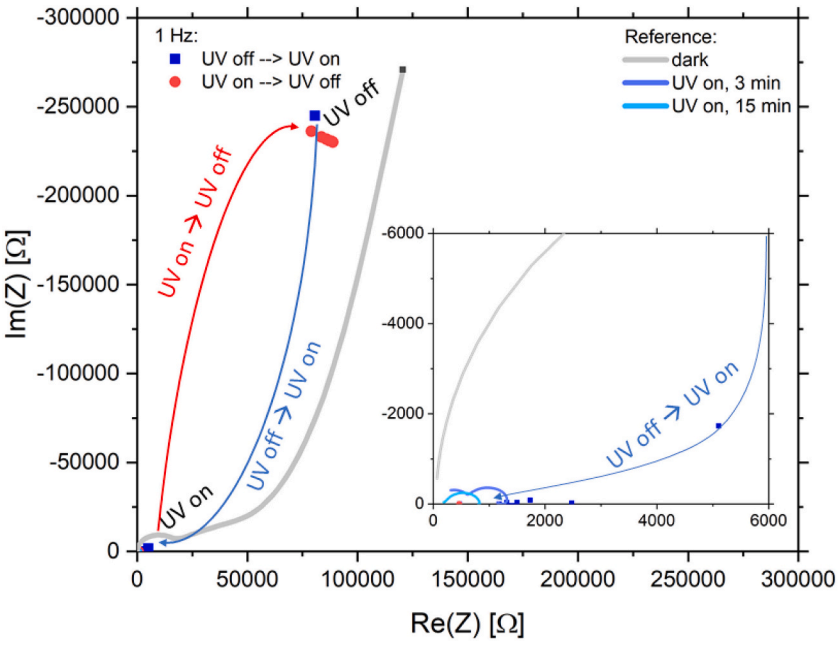

Fig. 9. EIS measurements of a LSCr10/STO cell at 350 °C in air at only 1 Hz for a better time resolution (the grey reference line represents the full spectrum in dark from Fig. 8). The process of switching the UV light (λ = 365 nm) on leads to lower resistances (i.e. 1 order of magnitude) within the time resolution of 1 s (blue squares). Under UV light, there is a slight, but steady decrease in resistance. Upon switching off the UV light, a very fast increase in resistance (within 1 s) is observed (red circles). (For interpretation of the references to color in this figure legend, the reader is referred to the web version of this article.)

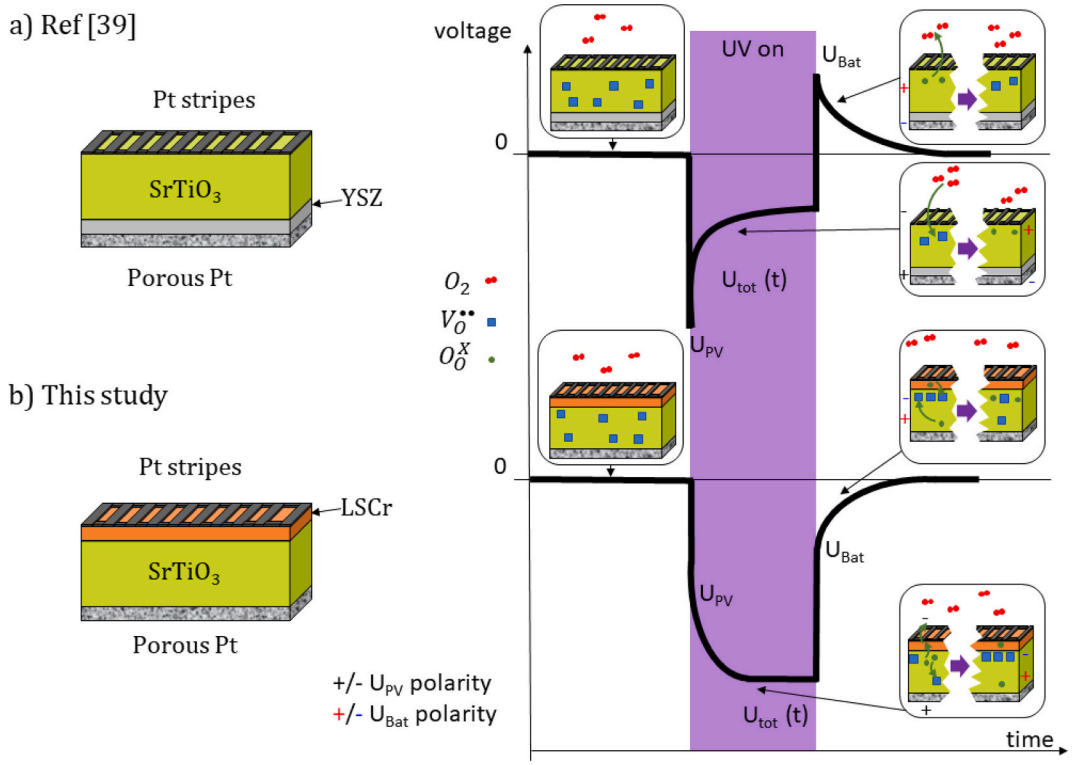

Fig. 10. Schematic representation of a sample with Pt stripes on top of an STO single crystal and a YSZ bottom layer as an electrolyte used in Ref. [39] (a) as well as a sample with a LSCr top layer on an STO single crystal (b). On the right hand side of each sample, the respective voltage-time curve is sketched, highlighting the time dependent processes under UV light. The polarity of the respective voltages, U_{PV} and U_{Bat}, are indicated.

yet. However, the exact validation requires many further studies and is beyond the scope of this paper; it is the topic of ongoing and future work.

With this in mind, we can address the difference in the processes leading to different timescales for photovoltage and photocurrent. Firstly, two different processes occur under UV light: i) change in oxygen chemical potential (addressed in this section), which occurs in both open and short circuit, and ii) stoichiometry polarization occurring only in the short circuit case. Secondly, the length scales, in which change in oxygen stoichiometry affects the result, differ for photovoltage and photocurrent. For photovoltage, only illuminated region of the STO (several μm) close to the interface, thereby affecting the space charge zone (few nm) and Fermi level at the interface, defines the outcome. However, the resistance of the whole STO single crystal (0.5 mm) is relevant for the measured short circuit photocurrent.

4. Conclusion

Heterojunctions of $SrTiO_3$ with semi-transparent thin films of different LSCr compositions or Au provide high photovoltages up to more than 1 V at 350 °C. The underlying effect seems to be very robust as both metals and ceramic materials work as a top layer, provided sufficient transparency of the thin film is given. The typically hole depleted space charges of the Schottky contact at the STO/top layer interfaces are responsible for the photovoltaic effects. When measuring the current of operating cells, a strong self-enhancing effect due to stoichiometry polarization in the STO single crystal is found. This may increase the current by orders of magnitude while leaving the open circuit photovoltage at its high value. Electrochemical impedance spectroscopy revealed details of the processes under UV light. Two processes under UV light could be identified: Immediately "switching off" the resistance of the space charge region and a continuous drop of the resistance of bulk STO due to stoichiometry polarization. A surprising time dependence of the photovoltage and its slow decay in dark is associated with compositional changes in illuminated STO due to formation of modified oxygen quasi-chemical potentials therein.

Declaration of Competing Interest

Maximilian Morgenbesser reports financial support was provided by EU Horizon 2020- No. 824072 - Harvestore.

Acknowledgements

The authors thankfully acknowledge the European Union's Horizon 2020 research and innovation program under grant agreement No. 824072 for the financial support. We thank M. Stchakovsky (Horiba Scientific) for support on SE measurements. SEM measurements were carried out using facilities at the University Service Centre for Transmission Electron Microscopy, Vienna University of Technology, Austria.

References

[1] A.W. Blakers, A. Wang, A.M. Milne, J. Zhao, M.A. Green, 22.8% efficient silicon solar cell, Appl. Phys. Lett. 55 (13) (1989) 1363–1365.
[2] P.P. Boix, S. Agarwala, T.M. Koh, N. Mathews, S.G. Mhaisalkar, Perovskite solar cells: beyond methylammonium lead iodide, J. Phys. Chem. Lett. 6 (5) (2015) 898–907.
[3] D.E. Carlson, C.R. Wronski, Amorphous silicon solar cell, Appl. Phys. Lett. 28 (11) (1976) 671–673.
[4] M.A. Green, The path to 25% silicon solar cell efficiency: history of silicon cell evolution, Prog. Photovolt. Res. Appl. 17 (3) (2009) 183–189.
[5] M.A. Green, E.D. Dunlop, J. Hohl-Ebinger, M. Yoshita, N. Kopidakis, A.W.Y. Ho-Baillie, Solar cell efficiency tables (version 55), Prog. Photovolt. Res. Appl. 28 (1) (2020) 3–15.
[6] N.K. Noel, S.D. Stranks, A. Abate, C. Wehrenfennig, S. Guarnera, A.-A. Haghighirad, A. Sadhanala, G.E. Eperon, S.K. Pathak, M.B. Johnston, A. Petrozza, L.M. Herz, H.J. Snaith, Lead-free organic–inorganic tin halide perovskites for photovoltaic applications, Energy Environ. Sci. 7 (9) (2014) 3061–3068.
[7] C. Strümpel, M. McCann, G. Beaucarne, V. Arkhipov, A. Slaoui, V. Švrček, C. del Cañizo, I. Tobias, Modifying the solar spectrum to enhance silicon solar cell efficiency—an overview of available materials, Sol. Energy Mater. Sol. Cells 91 (4) (2007) 238–249.
[8] R. Wang, M. Mujahid, Y. Duan, Z.-K. Wang, J. Xue, Y. Yang, A review of perovskites solar cell stability, Adv. Funct. Mater. 29 (47) (2019) 1808843.
[9] S. Rühle, A.Y. Anderson, H.-N. Barad, B. Kupfer, Y. Bouhadana, E. Rosh-Hodesh, A. Zaban, All-oxide photovoltaics, J. Phys. Chem. Lett. 3 (24) (2012) 3755–3764.
[10] T. Dittrich, V. Duzhko, F. Koch, V. Kytin, J. Rappich, Trap-limited photovoltage in ultrathin metal oxide layers, Phys. Rev. B 65 (15) (2002) 155319.
[11] J. Herion, E.A. Niekisch, G. Scharl, Investigation of metal oxide/cuprous oxide heterojunction solar cells, Solar Energy Mater. 4 (1) (1980) 101–112.
[12] R.J. Iwanowski, D. Trivich, Enhancement of the photovoltaic conversion efficiency in Cu/Cu_2O schottky barrier solar cells by H^+ ion irradiation, Phys. Status Solidi A **95** (2) (1986) 735–741.
[13] A.E. Rakhshani, Preparation, characteristics and photovoltaic properties of cuprous oxide—a review, Solid State Electron. 29 (1) (1986) 7–17.
[14] B.P. Rai, Cu_2O solar cells: a review, Solar Cells 25 (3) (1988) 265–272.
[15] J. Katayama, K. Ito, M. Matsuoka, J. Tamaki, Performance of Cu_2O/ZnO solar cell prepared by two-step electrodeposition, J. Appl. Electrochem. 34 (7) (2004) 687–692.
[16] T. Minami, Y. Nishi, T. Miyata, J.-i. Nomoto, High-efficiency oxide solar cells with ZnO/Cu_2O heterojunction fabricated on thermally oxidized Cu_2O sheets, Appl. Phys. Express 4 (6) (2011), 062301.
[17] Y. Nishi, T. Miyata, T. Minami, Effect of inserting a thin buffer layer on the efficiency in n-ZnO/p-Cu_2O heterojunction solar cells, J. Vac. Sci. Technol. A **30** (4) (2012) 04D103.
[18] D. Li, C.-J. Chien, S. Deora, P.-C. Chang, E. Moulin, J.G. Lu, Prototype of a scalable core–shell Cu_2O/TiO_2 solar cell, Chem. Phys. Lett. 501 (4) (2011) 446–450.
[19] K.P. Musselman, A. Wisnet, D.C. Iza, H.C. Hesse, C. Scheu, J.L. MacManus-Driscoll, L. Schmidt-Mende, Strong efficiency improvements in ultra-low-cost inorganic nanowire solar cells, Adv. Mater. 22 (35) (2010) E254–E258.
[20] K.P. Musselman, A. Marin, A. Wisnet, C. Scheu, J.L. MacManus-Driscoll, L. Schmidt-Mende, A novel buffering technique for aqueous processing of zinc oxide nanostructures and interfaces, and corresponding improvement of electrodeposited ZnO-Cu_2O photovoltaics, Adv. Funct. Mater. 21 (3) (2011) 573–582.
[21] K.P. Musselman, A. Marin, L. Schmidt-Mende, J.L. MacManus-Driscoll, Incompatible length scales in nanostructured Cu_2O solar cells, Adv. Funct. Mater. 22 (10) (2012) 2202–2208.
[22] J. Cui, U.J. Gibson, A simple two-step electrodeposition of Cu_2O/ZnO Nanopillar solar cells, J. Phys. Chem. C 114 (14) (2010) 6408–6412.
[23] S. Nakashima, T. Uchida, D. Nakayama, H. Fujisawa, M. Kobune, M. Shimizu, Bulk photovoltaic effect in a $BiFeO_3$ thin film on a $SrTiO_3$ substrate, Jpn. J. Appl. Phys. **53** (9S) (2014) 09PA16.
[24] S.Y. Yang, L.W. Martin, S.J. Byrnes, T.E. Conry, S.R. Basu, D. Paran, L. Reichertz, J. Ihlefeld, C. Adamo, A. Melville, Y.-H. Chu, C.-H. Yang, J.L. Musfeldt, D. G. Schlom, J.W.A. III, R. Ramesh, Photovoltaic effects in $BiFeO_3$, Appl. Phys. Lett. 95 (6) (2009), 062909.
[25] R.A. Rani, A.S. Zoolfakar, A.S. Ismail, S.S.A. Karim, M.H. Mamat, M. Rusop, High sensitivity ultra-violet photosensor based on nanostructured Nb_2O_5, AIP Conf. Proc. 2151 (1) (2019), 020031.
[26] X. Fang, L. Hu, K. Huo, B. Gao, L. Zhao, M. Liao, P.K. Chu, Y. Bando, D. Golberg, New ultraviolet photodetector based on individual Nb_2O_5 nanobelts, Adv. Funct. Mater. 21 (20) (2011) 3907–3915.
[27] K. Ozel, A. Atilgan, N.E. Koksal, A. Yildiz, A route towards enhanced UV photoresponse characteristics of SnO_2/p-Si based heterostructures by hydrothermally grown nanorods, J. Alloys Compd. 849 (2020) 156628.
[28] Y. Chen, C. Zhu, M. Cao, T. Wang, Photoresponse of SnO_2nanobelts grown in situ on interdigital electrodes, Nanotechnology 18 (28) (2007) 285502.
[29] N. Takubo, Y. Muraoka, Z. Hiroi, Conductivity switching by ultraviolet light in tin dioxide thin films, Appl. Phys. Express 2 (2009), 045501.
[30] N. Takubo, Y. Muraoka, Z. Hiroi, Effect of UV light irradiation in SnO_2 thin film, J. Phys. Conf. Ser. 148 (2009), 012025.
[31] M.-H. Huang, J.-Y. Xia, Y.-M. Xi, C.-X. Ding, Study on photochromism in $SrTiO_3$:Fe ceramic powder, J. Eur. Ceram. Soc. 17 (14) (1997) 1761–1765.
[32] F. Rossella, P. Galinetto, G. Samoggia, V. Trepakov, L. Jastrabik, Photoconductivity and the structural phase transition in $SrTiO_3$, Solid State Commun. 141 (2) (2007) 95–98.
[33] S. Mehra, S. Bishnoi, L. Goswami, G. Gupta, A.K. Srivastava, S. Narain Sharma, Detailed chemical mechanism of the phase transition in nano-$SrTiO_3$ perovskite with visible luminescence, Inorg. Chem. Commun. 120 (2020) 108125.
[34] S. Zhang, D. Guo, M. Wang, M.S. Javed, C. Hu, Magnetism in $SrTiO_3$ before and after UV irradiation, Appl. Surf. Sci. 335 (2015) 115–120.
[35] H. Katsu, H. Tanaka, T. Kawai, Anomalous photoconductivity in $SrTiO_3$, Jpn. J. Appl. Phys. **39** (2000) 2657–2658. Part 1, No. 5A.
[36] F.V.E. Hensling, D.J. Keeble, J. Zhu, S. Brose, C. Xu, F. Gunkel, S. Danylyuk, S. S. Nonnenmann, W. Egger, R. Dittmann, UV radiation enhanced oxygen vacancy formation caused by the PLD plasma plume, Sci. Rep. 8 (1) (2018) 8846.
[37] R. Merkle, R. Souza, J. Maier, Optically tuning the rate of stoichiometry changes: surface-controlled oxygen incorporation into oxides under UV irradiation, Angew. Chem. **40** (2001) 2126–2129 (International ed. in English).
[38] A. Viernstein, M. Kubicek, M. Morgenbesser, G. Walch, G.C. Brunauer, J. Fleig, High-temperature photochromism of Fe-doped SrTiO3 caused by UV-induced bulk stoichiometry changes, Adv. Funct. Mater. 29 (23) (2019) 1900196.
[39] G. Walch, B. Rotter, G.C. Brunauer, E. Esmaeili, A.K. Opitz, M. Kubicek, J. Summhammer, K. Ponweiser, J. Fleig, A solid oxide photoelectrochemical cell with UV light-driven oxygen storage in mixed conducting electrodes, J. Mater. Chem. A 5 (4) (2017) 1637–1649.
[40] K. Zhao, Y. Huang, Q. Zhou, K.-J. Jin, H. Lu, M. He, B. Cheng, Y. Zhou, Z. Chen, G. Yang, Ultraviolet photovoltage characteristics of $SrTiO_{3-\delta}$□Si heterojunction, Appl. Phys. Lett. 86 (22) (2005) 221917.
[41] J. Wen, H. Guo, J. Xing, H. Lü, K.-J. Jin, M. He, G. Yang, High-sensitivity photovoltage based on the interfacial photoelectric effect in the $SrTiO_{3-\delta}$/Si heterojunction, Sci. China Phys. Mech. Astron. 53 (11) (2010) 2080–2083.
[42] F.X. Hao, C. Zhang, X. Liu, Y.W. Yin, Y.Z. Sun, X.G. Li, Photovoltaic effect in $YBa_2Cu_3O_{7-\delta}$/Nb-doped $SrTiO_3$ heterojunctions, Appl. Phys. Lett. 109 (13) (2016) 131104.
[43] H. Liu, K. Zhao, N. Zhou, H. Lu, M. He, Y. Huang, K.-J. Jin, Y. Zhou, G. Yang, S. Zhao, A. Wang, W. Leng, Photovoltaic effect in micrometer-thick perovskite-type oxide multilayers on Si substrates, Appl. Phys. Lett. 93 (17) (2008) 171911.
[44] T. Muramatsu, Y. Muraoka, Z. Hiroi, Photocarrier injection and the I–V characteristics of $La_{0.8}Sr_{0.2}MnO_3/SrTiO_3$:Nb heterojunctions, Solid State Commun. 132 (5) (2004) 351–354.
[45] C. Wang, K.-j. Jin, R.-q. Zhao, H.-b. Lu, H.-z. Guo, C. Ge, M. He, C. Wang, G.-z. Yang, Ultimate photovoltage in perovskite oxide heterostructures with critical film thickness, Appl. Phys. Lett. 98 (18) (2011) 181101.

[46] C. Wang, Z.F. Li, X.M. Chen, J.M. Liu, Z.M. Liu, H.Y. Cui, Y. Yang, W. Lu, Study of carrier behavior in $La_{0.9}Ba_{0.1}MnO_{3-\delta}$/$SrTiO_3$:Nb p-n heterojunction, Thin Solid Films 516 (12) (2008) 4282–4287.
[47] J.F. Wang, D. Cao, Y. Zhou, X.Y. Wang, Z.W. Jiao, J. Gao, Series resistance effects in $La_{0.5}Ca_{0.5}MnO_3$/$SrTiO_3$:Nb(001) heterojunctions, J. Phys. D. Appl. Phys. 48 (38) (2015) 385104.
[48] K. Wang, W. Gao, H.W. Zheng, F.Z. Li, M.S. Zhu, G. Yang, G.T. Yue, Y.K. Liu, R. K. Zheng, Heteroepitaxial growth of Cu_2O films on Nb-$SrTiO_3$ substrates and their photovoltaic properties, Ceram. Int. 43 (18) (2017) 16232–16237.
[49] S. Wang, H. Li, K. Zhao, S. Zhao, M. Chen, J. Chen, J. Wang, G. Fu, Rectifying and photovoltage characteristics of $Bi_2Sr_2Co_2O_y$/Nb-doped $SrTiO_3$ heterojunction, Applied Physics A 105 (2) (2011) 407–410.
[50] Z.J. Yue, K. Zhao, S.Q. Zhao, Z.Q. Lu, X.M. Li, H. Ni, A.J. Wang, Thickness-dependent photovoltaic effects in miscut Nb-doped $SrTiO_3$ single crystals, J. Phys. D. Appl. Phys. 43 (1) (2009), 015104.
[51] S.G. Zhao, J.F. Cheng, T. Zhang, Y. Xie, X.L. Yan, W. Liu, J.Y. Wang, K.X. Jin, Photovoltaic effect in heterojunction composed of charge-ordering $Pr_{0.75}Na_{0.25}MnO_3$ and Nb–$SrTiO_3$, Phys. B Condens. Matter 454 (2014) 42–44.
[52] S.G. Zhao, A. Gu, X.L. Yan, L.M. Hao, Y. Xie, T. Zhang, K.X. Jin, Transport and photoresponse properties in $Pr_{0.5}Ca_{0.5}CoO_3$/Nb-$SrTiO_3$ heterostructure, EPL (Europhysics Letters) **108** (6) (2014) 67007.
[53] F. Horikiri, T. Ichikawa, L.Q. Han, A. Kaimai, K. Yashiro, H. Matsumoto, T. Kawada, J. Mizusaki, Nb-doped $SrTiO_3$-based high-temperature schottky solar cells, Jpn. J. Appl. Phys. 44 (11) (2005) 8023–8026.
[54] J. Dho, Electrode size dependent I–V characteristics and photovoltaic effect in the oxide p–n junctions $Pr_{0.7}Ca_{0.3}MnO_3$/Nb:$SrTiO_3$ and $La_{0.7}Ca_{0.3}MnO_3$/Nb:$SrTiO_3$, Solid State Commun. 150 (45) (2010) 2243–2247.
[55] G.C. Brunauer, B. Rotter, G. Walch, E. Esmaeili, A.K. Opitz, K. Ponweiser, J. Summhammer, J. Fleig, UV-light-driven oxygen pumping in a high-temperature solid oxide photoelectrochemical cell, Adv. Funct. Mater. 26 (1) (2016) 120–128.
[56] D.J. Keeble, S. Wicklein, L. Jin, C.L. Jia, W. Egger, R. Dittmann, Nonstoichiometry accommodation in $SrTiO_3$ thin films studied by positron annihilation and electron microscopy, Phys. Rev. B 87 (19) (2013) 195409.
[57] A. Ojeda-G-P, M. Döbeli, T. Lippert, Influence of plume properties on thin film composition in pulsed laser deposition, Adv. Mater. Interfaces 5 (18) (2018) 1701062.
[58] A. Tebano, E. Fabbri, D. Pergolesi, G. Balestrino, E. Traversa, Room-temperature Giant persistent photoconductivity in $SrTiO_3$/$LaAlO_3$ heterostructures, ACS Nano 6 (2) (2012) 1278–1283.
[59] R. Gurwitz, R. Cohen, I. Shalish, Interaction of light with the ZnO surface: Photon induced oxygen "breathing," oxygen vacancies, persistent photoconductivity, and persistent photovoltage, J. Appl. Phys. 115 (3) (2014), 033701.
[60] Y.-C. Ho, M.N.F. Hoque, E. Stoneham, J. Warzywoda, T. Dallas, Z. Fan, Reduction of oxygen vacancy related traps in TiO_2 and the impacts on hybrid perovskite solar cells, J. Phys. Chem. C 121 (43) (2017) 23939–23946.
[61] M.D. Scafetta, Y.J. Xie, M. Torres, J.E. Spanier, S.J. May, Optical absorption in epitaxial $La_{1-x}Sr_xFeO_3$ thin films, Appl. Phys. Lett. 102 (8) (2013), 081904.
[62] S. Mildner, J. Hoffmann, P.E. Blöchl, S. Techert, C. Jooss, Temperature- and doping-dependent optical absorption in the small-polaron system $Pr_{1-x}Ca_xMnO_3$, Phys. Rev. B 92 (3) (2015), 035145.
[63] L.V. Nomerovannaya, A.A. Makhnëv, A.Y. Rumyantsev, Evolution of the optical properties of single-crystal $La_{1-x}Sr_xMnO_3$, Phys. Solid State 41 (8) (1999) 1322–1326.
[64] R. Raffaelle, H.U. Anderson, D.M. Sparlin, P.E. Parris, Transport anomalies in the high-temperature hopping conductivity and thermopower of Sr-doped La(Cr,Mn) O_3, Phys. Rev. B 43 (10) (1991) 7991–7999.
[65] M.S.R. Khan, A. Reza, Optical and electrical properties of optimized thin gold films as top layer of MIS solar cells, Applied Physics A 54 (2) (1992) 204–207.
[66] P.V. Sushko, L. Qiao, M. Bowden, T. Varga, G.J. Exarhos, F.K. Urban, D. Barton, S. A. Chambers, Multiband optical absorption controlled by lattice strain in thin-film $LaCrO_3$, Phys. Rev. Lett. 110 (7) (2013), 077401.
[67] K.H.L. Zhang, Y. Du, A. Papadogianni, O. Bierwagen, S. Sallis, L.F.J. Piper, M. E. Bowden, V. Shutthanandan, P.V. Sushko, S.A. Chambers, Perovskite Sr-doped $LaCrO_3$ as a new p-type transparent conducting oxide, Adv. Mater. 27 (35) (2015) 5191–5195.
[68] A. Frye, R.H. French, D.A. Bonnell, Optical properties and electronic structure of oxidized and reduced single-crystal strontium titanate, Z. Met. 94 (3) (2003) 226–232.
[69] M. Capizzi, A. Frova, Optical gap of strontium titanate (deviation from urbach tail behavior), Phys. Rev. Lett. 25 (18) (1970) 1298–1302.
[70] A. Rothschild, W. Menesklou, H.L. Tuller, E. Ivers-Tiffée, Electronic structure, defect chemistry, and transport properties of $SrTi_{1-x}Fe_xO_{3-y}$ solid solutions, Chem. Mater. 18 (16) (2006) 3651–3659.
[71] R. Waser, T. Baiatu, K.-H. Härdtl, dc electrical degradation of perovskite-type titanates: I, ceramics, J. Am. Ceram. Soc. 73 (6) (1990) 1645–1653.
[72] S. Rodewald, N. Sakai, K. Yamaji, H. Yokokawa, J. Fleig, J. Maier, The effect of the oxygen exchange at electrodes on the high-voltage Electrocoloration of Fe-doped $SrTiO_3$ single crystals: a combined SIMS and microelectrode impedance study, J. Electroceram. 7 (2) (2001) 95–105.
[73] S. Rodewald, J. Fleig, J. Maier, Resistance degradation of iron-doped strontium titanate investigated by spatially resolved conductivity measurements, J. Am. Ceram. Soc. 83 (8) (2000) 1969–1976.
[74] S. Rodewald, J. Fleig, J. Maier, Measurement of conductivity profiles in acceptor-doped strontium titanate, J. Eur. Ceram. Soc. 19 (6) (1999) 797–801.
[75] T. Baiatu, R. Waser, K.-H. Härdtl, Dc electrical degradation of perovskite-type titanates: III, a model of the mechanism, J. Am. Ceram. Soc. 73 (6) (1990) 1663–1673.
[76] R.A. De Souza, J. Fleig, J. Maier, O. Kienzle, Z. Zhang, W. Sigle, M. Rühle, Electrical and structural characterization of a low-angle tilt grain boundary in iron-doped strontium titanate, J. Am. Ceram. Soc. 86 (6) (2003) 922–928.
[77] J. Maier, Mass transport in the presence of internal defect reactions—concept of conservative ensembles: III, trapping effect of dopants on chemical diffusion, J. Am. Ceram. Soc. 76 (5) (1993) 1223–1227.
[78] R.A. De Souza, V. Metlenko, D. Park, T.E. Weirich, Behavior of oxygen vacancies in single-crystal $SrTiO_3$: equilibrium distribution and diffusion kinetics, Phys. Rev. B 85 (17) (2012) 174109.
[79] R.A. De Souza, Oxygen diffusion in $SrTiO_3$ and related perovskite oxides, Adv. Funct. Mater. 25 (40) (2015) 6326–6342.